

Feasibility of the use of nonlinear solitary waves for the nondestructive measurement of Young's modulus of rocks and compacted materials

Juan P. Villacreses^{a,b}, Bernardo Caicedo^{a,*}, Silvia Caro^a, Fabricio Yépez^b

^a Universidad de los Andes, Carrera 1E #19A-40, Mario Laserna (ML) Building, Piso 6, Department of Civil and Environmental Engineering, Bogotá 111711, Colombia

^b Universidad San Francisco de Quito, Colegio de Ciencias e Ingenierías, Via Interoceánica y Diego de Robles, Quito, Ecuador

ARTICLE INFO

Keywords:

Nonlinear solitary waves
Young's modulus
Compaction control
Nondestructive test

ABSTRACT

This article describes the development of a new device to measure the Young's modulus of geomaterials. This device bases its operation on the propagation of nonlinear solitary waves along a chain full of spheres. The chain is placed vertically on the sample's surface, and then an incident wave is generated at its top. The pulse travels through the chain of spheres from top to bottom, generating a reflected wave as a result of the interaction between the last element and the material tested. The time-lapse between the incident and reflected waves, measured using a piezoelectric load cell inserted in the middle of the chain of spheres, allows the estimation of the Young's modulus of the sample through a numerical model. The usefulness of the device is demonstrated in control samples of known elastic properties, rocks, and compacted soils. Besides, this paper proposes a modification of the device, which consists of placing a metal cylinder instead of the last sphere of the chain; This modification improves the results obtained when analyzing soft soils. The results show that Young's moduli calculated by the developed device are equivalent to the modulus measured by alternative tests. This device could become a useful nondestructive test for measuring Young's modulus of subgrade materials.

Introduction

The serviceability of most geotechnical structures and their response to vibratory loads, earthquakes, or moving wheels depend on the elastic properties of the materials measured at low levels of strain. A particular case is the construction of road structures that requires the measurement of the elastic properties continuously, a necessity that requires the development of simple, inexpensive, and nondestructive procedures.

Over the years, many laboratory tests have been developed to characterize the mechanical response of soils under dynamic loads; some of among them includes the triaxial test, the bender element test, the resonant column test, and the simple cyclic shear test.

The triaxial cyclic test is a compression test that applies confinement around the sample. The apparatus imposes a controlled axial cyclic stress or strain and records load or displacement. These measures allow calculating Young's dynamic modulus in different ranges of strain [1]. Usually, strain measurements are performed outside the triaxial chamber, leading to errors in the calculation of the modulus. To cope with this problem, advanced triaxial devices that improve the accurate measurement of strain by placing displacement transducers within the triaxial chamber have been developed. These apparatuses allow 10^{-6}

precision in the measured strains. One way to achieve such precision is by using a set of strain gauges glued to a small metallic beam that deflects when the load is applied [2,3]. The transducer is positioned longitudinally, and its deflection due to bending allows the displacement to be calculated.

Bender extender element test uses wave propagation theory, which establishes a relationship between wave velocities (*i.e.*, P or S wave velocity), sample density, and elastic constants [4]. The mechanical waves are produced by a piezoelectric ceramic inserted at the base of the sample. These waves travel through the sample and hit another ceramic piezoelectric element inserted at the top. As this test is non-destructive, it allows an unlimited number of repetitive tests. Besides, piezoelectric elements can be installed in a wide variety of devices, such as the resonant column and the triaxial apparatus. However, determining the time of arrival of the mechanical wave at the piezoelectric receiver remains an unsolved problem, and different procedures to estimate this time lead to different Young's modulus results [5].

The cyclic simple shear test applies controlled shear and vertical stresses to a sample placed within a rigid membrane [6]. Simple shear equipment can measure deformations ranging from 10^{-5} to 4×10^{-4} [7]. However, the interaction between the soil and the membrane

* Corresponding author.

E-mail addresses: jp.villacreses@uniandes.edu.co (J.P. Villacreses), bcaicedo@uniandes.edu.co (B. Caicedo), scaro@uniandes.edu.co (S. Caro), fyeperez@usfq.edu.ec (F. Yépez).

Nomenclature	
a	Radius of the cylindrical element, or the contact area of a spherical element
A	Coefficient of proportionality for the Hertzian contact
A_{bott}	Coefficient for the contact at the bottom of the element
A_{cyl}	Area of the cross section of the cylindrical element
A_m	Coefficient for the contact between a sphere and the material under testing
A_{sph}	Coefficient for the contact between spheres
A_{top}	Coefficient for the contact at the top of the element
A_{ws}	Coefficient for the contact between spheres and the load cell
d	Indentation for a contact between a circular area and the tested material
E	Young modulus of a sphere
E^*	Equivalent Young modulus
E_{cr}	Modified Young modulus accounting for the asperities
E_{cy}	Young modulus of the cylindrical element
E_m	Young modulus of the material under testing
E_{ws}	Young modulus of the sensing element
e	Coefficient of restitution for the collision between steel spheres
F	Contact force between elements
F_c	Force between a circular flat surface and an elastic medium
g	Acceleration of gravity
m_i	Mass of the element i
R	Radius of the spheres
TOF	Time Of Flight, time-lapse between the incident and the reflected waves, measured peak to peak
u_i	Displacement of the element i
V_i	Velocity of the element i
V_{oi}	Velocity of the impactor when it strikes the first sphere
V_{of}	Velocity of the impactor after it strikes the first sphere
W	Contact force on the circular area
α	Empirical constant accounting for the asperities of the contact cylinder-sample
β	Empirical constant accounting for the asperities of the contact cylinder-sample
ε_c	Contact strain below a sphere or the symmetry axis of the flat surface of a cylinder
δ	Depending on the type of contact: (a) relative displacement between the center of two spheres in contact, or (b) the displacement between the center of a sphere and a flat surface, or (c) the penetration into the material of a flat surface of a cylinder
δ_0	Pre-compression displacement caused by the self-weight of the portion of the chain that is above the analyzed element
μ	Poisson ratio of the spheres
μ_{cyl}	Poisson ratio of the cylindrical element
μ_m	Poisson ratio of the material under testing
μ_s	Poisson ratio of the sensing element

particles can alter the results [8]. Furthermore, there is evidence that the stresses are not uniformly distributed over the sample, which is one of the main assumptions of the procedure [9].

The Resonant Column test is used to measure the elastic properties and the damping ratio of soil samples. In this test, the resonance frequency of the system device-sample is measured when a torsional harmonic signal is applied, allowing the elastic constants of the sample to be calculated [10]. Another property that can be measured with this test is the damping ratio. This property is computed as the logarithmic decay of a given impulse when one side of the sample is left unconstrained, and the material is assumed to behave as a Kelvin-Voigt element. However, the practicality of this test is overshadowed by the difficulties in coupling the sample to the apparatus [11].

Despite the advances in experimental procedures applied to soil dynamics, laboratory tests are not always applicable to all projects, and each procedure is applicable only under specific conditions. Furthermore, these tests use trimmed samples, where the mechanical properties can be altered. Because of the limitations of the available tests, it is necessary to have simple procedures in the professional practice that can estimate elastic parameters in the design stages or during the construction process. This need can be overcome by developing new procedures or complementary devices.

This paper uses a device based on the propagation of nonlinear solitary waves that was developed in [12], extending its usefulness to geomaterials. Solitary waves propagate through a chain of spheres that transmit only compression loads between them. When a pulse is applied at the top of this chain, a compression wave propagates to the bottom and travels backward when it hits the material placed at the bottom. The time-lapse between the incident and the reflected waves (measured peak to peak), denoted as TOF , or time of flight, permits to calculate the Young's modulus of the material through a numerical model [13,14]. Several studies have used solitary wave-based devices to measure Young's modulus of materials such as rubber, elastic solids, elastic hollow spheres, and composite beams [15,16,17,18,19]. However, even with the vast applicability of the device, there is little evidence of having been used in civil engineering materials [20].

The purpose of this work is to explore the applicability of nonlinear solitary wave devices to calculate Young's modulus of geomaterials (*i.e.*, rocks and compacted soils) at small strains. For this research, a nonlinear solitary wave device was constructed, and its proper operation was verified by comparing the experimental TOF measurements obtained using control samples of known elastic properties, with the results of a numerical model that simulates the operation of the device.

The experimental component of this study, regarding geomaterials, is carried out in two phases. The first phase includes measures on eleven rock samples and seventeen compacted soil samples. The results of these tests were compared with the results obtained by compression wave velocity tests. Nevertheless, during the first phase of experimentation, plastic deformations were identified, particularly when testing samples of soft compacted soils. Consequently, a second phase proposes an improvement of the device that consists of substituting the last element of the chain by a metallic cylinder. The usefulness of this modification is analyzed by testing eleven soil samples, and their results are compared with the elastic modulus measured using a dynamic shear rheometer.

The results of this research suggest that the proposed device could be applied in the laboratory or the field as an indirect technique to measure Young's modulus of geomaterials under low confining stresses, such as subgrades of road structures.

Theoretical considerations

Analysis of the propagation of solitary waves

As the contact between spheres is Hertzian [21], when an element of the chain is disturbed, a nonlinear strain wave travels through the arrangement of spheres. A theory that describes the propagation of nonlinear solitary waves through a chain of spheres was proposed in [22]; which combines Newton's second law with the Hertz contact theory.

The Hertz contact law provides a relationship between the contact force (F) between spherical particles, and the relative displacement between their centers (δ), using a coefficient of proportionality (A)

[23]. However, when the two elements are not in contact (*i.e.*, $\delta < 0$), the force acting on them is zero (Eq. (1)). Then the expression for the contact force is [16]:

$$\begin{cases} F = A\delta^{\frac{3}{2}}\delta \geq 0 \\ F = 0\delta < 0 \end{cases} \quad (1)$$

The value of A depends on the elastic properties of the elements and the shape of the solids in contact [21]. In this research, the coefficient of proportionality A can have three possible values, depending on the shape of the elements of the chain. Eq. (2) is used to compute the coefficient of proportionality when two spheres are in contact (A_{sph}), Eq. (3) is used to compute this coefficient when a sphere is in contact with a flat surface (A_{ws}), and Eq. (4) gives the constant A_m when a sphere and the medium tested are in contact. These equations use the Poisson's ratio (μ) and Young's modulus (E) of the spheres; the Poisson's ratio (μ_{ws}) and Young's modulus (E_{ws}) of the sensor placed in the middle of the chain, the Poisson's ratio (μ_m) and Young's modulus (E_m) of the tested material, and the radius of the spheres (R).

$$A_{sph} = \frac{2E}{3(1-\mu^2)} \left(\frac{R^2}{2R} \right)^{1/2} \quad (2)$$

$$A_{ws} = \frac{4}{3}\sqrt{R} \left(\frac{1-\mu^2}{E} + \frac{1-\mu_{ws}^2}{E_{ws}} \right)^{-1} \quad (3)$$

$$A_m = \frac{4}{3}\sqrt{R} \left(\frac{1-\mu^2}{E} + \frac{1-\mu_m^2}{E_m} \right)^{-1} \quad (4)$$

Fig. 1 allows identifying the proper equation to compute the proportionality constant A for the SSW experiment. For instance, when considering element 8, the constant for the upper contact is sphere-sphere, A_{sph} , whereas the contact between sphere 8 and element 9 is that of a sphere-flat surface, A_{ws} . The Young's modulus of the sensing element, E_{ws} , is calculated knowing the axial stiffness reported by the fabricant (*i.e.*, 2×10^9 N/m) and the cross-sectional area of the device. At the same time, its Poisson's ratio is assumed to be similar to that of the steel. The effect of such assumptions was evaluated by calculating the TOF by changing E_{ws} two and a half times the assumed value based on the data reported by the manufacturer, and also changing the Poisson's ratio from 0.1 to 0.4. The results show that when the sensor stiffness doubles, the TOF decreases 9.6 μ s, while when it decreases to half the manufacturer's value, the TOF increases 4.6 μ s. Also, changes in the Poisson's ratio result in TOF values of < 4 μ s. The results of these simulations show that both the Young's modulus and Poisson's ratio of the sensor have a small effect on the calculated TOF value. Nevertheless, it is expected that these variations would have a nonnegligible effect when testing materials of high Young's modulus.

It is essential to keep in mind that the Hertz's contact law relies on two assumptions. First, the maximum contact stress must be smaller than the elastic limit of both materials in contact and, second, that the contact time of the force must be longer than the natural period of each element of the chain [24].

On the other hand, Newton's second law permits to obtain one motion equation for each element of the chain. The motion's equation of each element denoted with the sub-index ' i ', as shown in **Fig. 1**, takes in to account the contact forces between the elements, its self-weight, the displacement induced in the chain due to the effect of the gravity (δ_{0i}), and the inertial force. In Eqs. (5)–(7), u_i is used to represent the displacement of the center of the element ' i '. Note that Eq. (5) has fewer terms than Eqs. (6) and (7), because this equation represents the motion of the first element that does not have an upper element to interact with. Eq. (6) represents the motion of the second to the sixteenth element (' i ', from 2 to 16), and Eq. (7) describes the motion of the last sphere ($i = 17$), which is in contact with the sample under testing. Contact type between the analyzed element and the top and bottom elements is characterized in these equations by the constants A_{top} or

A_{bott} . These constants are computed using Eq. (2) or (3), while the element's weight is computed by multiplying its mass (m_i) by the acceleration of the gravity (g). Finally, the inertial force is computed as the product of the mass of the element and its acceleration (\ddot{u}_i).

$$m_i \ddot{u}_i = -A_{sph} (\delta_{01} - u_2 + u_1)^{\frac{3}{2}} + m_i g \quad (5)$$

$$m_i \ddot{u}_i = A_{top} (\delta_{0i-1} - u_i + u_{i-1})^{\frac{3}{2}} - A_{bott} (\delta_{0i} - u_{i+1} + u_i)^{\frac{3}{2}} + m_i g \quad (6)$$

$$m_{17} \ddot{u}_{17} = A_{sph} (\delta_{016} - u_{17} + u_{16})^{\frac{3}{2}} - A_m (\delta_{017} - u_{17})^{\frac{3}{2}} + m_{17} g \quad (7)$$

where δ_{0i} is the relative displacement between particles i and $i-1$ due to gravity (g), which is given by the following expression, Eq. (8) [15]:

$$\delta_{0i} = \left(\frac{\sum_{i=1}^{i-1} m_i g}{A_{sph}} \right)^{2/3} \quad (8)$$

The system composed by Eqs. (5) to (7) is then transformed into a set of simultaneous first-order differential equations. This change of variables is achieved by changing the acceleration of each element with their first derivative of the velocity respect to time, \dot{V}_i . Then, the new set of equations (*i.e.*, Eq. (9) with "I" ranging from 1 to 17) describe the relation of the first derivative of the displacement with respect to time (\dot{u}_i) and the velocity of the element (V_i).

$$\dot{u}_i = V_i \quad (9)$$

$$\dot{V}_1 = \frac{1}{m_1} (-A_{sph} (\delta_{01} - u_2 + u_1)^{\frac{3}{2}} + m_i g) \quad (10)$$

$$\dot{V}_i = \frac{1}{m_i} (A_{top} (\delta_{0i-1} - u_i + u_{i-1})^{\frac{3}{2}} - A_{bott} (\delta_{0i} - u_{i+1} + u_i)^{\frac{3}{2}} + m_i g) \quad (11)$$

$$\dot{V}_{17} = \frac{1}{m_{17}} (A_{sph} (\delta_{016} - u_{17} + u_{16})^{\frac{3}{2}} - A_m (\delta_{017} - u_{17})^{\frac{3}{2}} + m_{17} g) \quad (12)$$

The initial conditions for Eqs. (9) to (12) are: $u_i = V_i$, $\dot{u}_{2to17} = 0$, and $\dot{V}_{1to17} = 0$. The initial velocity, V_1 , represents the strike produced on the top sphere by the spherical impactor. This velocity is computed using Eq. (13) that considers the coefficient of restitution (e) and Eq. (14) that

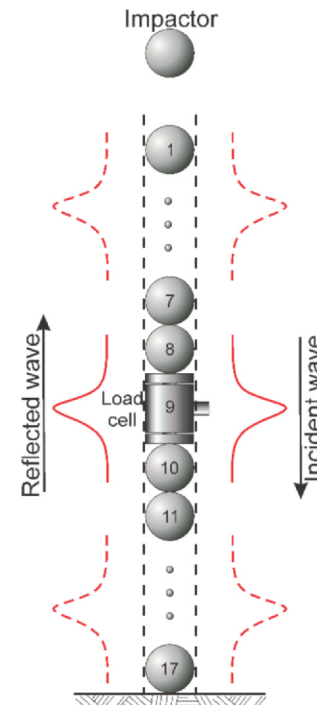


Fig. 1. Principle of operation of the proposed SSW.

considers the conservation of linear momentum of the collision of particles. The mass of the impactor is labeled as m_0 , while the initial and final collision velocity of the impactor are labeled as V_{0i} and V_{0f} . A value of $e = 0.7$ is selected for the coefficient of restitution based on suggested values for collisions of spherical elements [25].

$$e = \frac{V_1 - V_{0f}}{V_{0i}} \quad (13)$$

$$m_0 V_{0i} = m_0 V_{0f} + m_1 V_1 \quad (14)$$

The initial velocity of the impactor when striking the first sphere (*i.e.*, Eq. (15)) depends on its falling height (h) and the acceleration of the gravity (g), thus:

$$V_{0i} = \sqrt{2gh} \quad (15)$$

The simultaneous differential equations presented in Eqs. (9) to (12) can be solved numerically [13]. This solution permits to compute the time lag between the incident and the reflected wave in the load cell (*i.e.*, the TOF), which depends on Young's modulus of the material that is in contact with the last sphere of the chain. For the numerical simulation, the elastic constants of the metallic spheres are $E = 200$ GPa and $\mu = 0.29$ [14]. The values of the Young's modulus of the samples (*i.e.*, E_m) adopted in the simulations are in the range of 10 MPa to 10^3 MPa. These simulations are conducted using different values of Poisson's ratio (*i.e.*, $\mu_m = 0.1, 0.3$ and 0.5). The results of the numerical model permit to obtain a relationship between the TOF and Young's modulus of the sample. Subsequently, this relationship permits to estimate the Young's modulus of the material based on the experimental measurement of the TOF.

A modification of the device is proposed to overcome plastic deformation on soil samples. For this purpose, a cylinder of the same diameter and height of the spheres is placed as the last element of the chain. This modification allows spreading the stresses on a broader contact area, avoiding the development of plastic strains on the sample. Regarding the numerical model, this change requires substituting the Hertzian contact of the last element by a contact law applicable to a flat circular area [16]. Eq. (16) presents the relation of the contact force (F_c) and the indentation (d) of a cylindrical element penetrating in the elastic half-space. The contact force in this equation (F_c) depends on the radius of the cylinder (a) and the equivalent Young's modulus that results from the interaction between the contact material and the cylinder (E^*),

$$F_c = 2aE^*d \quad (16)$$

The equivalent Young's modulus (E^*) considers the elastic properties of the two elements in contact: Young's modulus and Poisson's ratio of the sample (*i.e.*, E_{cr} and μ_m), and of the cylindrical element (*i.e.*, E_{cyl} and μ_{cyl}), as

$$\frac{1}{E^*} = \frac{1 - \mu_m^2}{E_{cr}} + \frac{1 - \mu_{cyl}^2}{E_{cyl}} \quad (17)$$

On the other hand, the contact cylinder-sample is considered rough because of the asperities of the surface of the sample. For this kind of contact, a modified Young's modulus of the contact material (*i.e.*, E_{cr}) that considers the asperities of the surface was proposed in [27], leading to Eq. (18). In this equation, α and β are constants that depend on the asperities of the surface. For this research, $\alpha = 1.1 \times 10^{-1}$ and $\beta = 4.6 \times 10^{-1}$ were selected, according to the recommendations given in [27] for materials whose roughness is between $0.05 \mu\text{m}$ to $3 \mu\text{m}$, which agrees with the roughness suggested for soils samples [28].

$$\frac{E_{cr}}{E_m} = \beta \left(\frac{W}{E_m A_{cyl}} \right)^\alpha \quad (18)$$

To include this last modification in the numerical model, Eq. (12) is substituted by Eq. (19). As before, the new set of differential equations

is used to obtain a relationship between the TOF and Young's modulus of the sample, which permits to compute the Young's modulus of the sample based on the experimental measurements of the TOF.

$$\dot{V}_{17} = \frac{1}{m_{17}} \left(A_{Top} (\delta_{016} - u_{17} + u_{16})^{\frac{3}{2}} - F_c + m_{17} g \right) \quad (19)$$

Stress distribution beneath the contact area

The contact theory makes it possible to calculate the stress distribution under a sphere or a flat surface of a rigid cylinder [24]. In fact, based on the contact elements used in this study, Hertz's theory allows calculating the contact stress when the body is a sphere [23]. In contrast, Sneddon's theory provides the contact stress when the body corresponds to the flat surface of a cylinder [26].

According to Hertz [23], the contact between a sphere and a flat surface produces an elliptical stress distribution on the surface, which magnitude is given by

$$\sigma_z(r) = p_0 \left(1 - \frac{r^2}{a^2} \right)^{1/2} \quad (20)$$

where r is the radial distance measured from the symmetry axis to the point where the stress is calculated.

Following expressions give the maximum stress, p_0 , located on the symmetry axis, and the radius of the circular contact area a :

$$p_0 = \left(\frac{6F_c E^{*2}}{\pi^3 R^2} \right)^{1/3} \quad (21)$$

$$a = \left(\frac{3F_c R}{4E^*} \right)^{1/3} \quad (22)$$

On the other hand, when the element in contact is a cylinder, the mean contact pressure under its flat surface, p_m , is

$$p_m = \frac{F_c}{\pi a^2} \quad (23)$$

Leading to the following stress distribution

$$\sigma_z(r) = \frac{p_m}{2} \left(1 - \frac{r^2}{a^2} \right)^{-1/2} \quad (24)$$

Fig. 2a illustrates the distribution of vertical contact stresses produced by a unit load ($F_c = 1 \text{ N}$) when the contact bodies are spheres resting on materials of different equivalent Young's modulus or a cylinder. It is noticeable in this figure that, when the body in contact is a sphere, the contact area decreases, and the contact stress increases as the equivalent Young's modulus grows. However, despite the increase of the contact stress, the contact strain in the symmetry axis decreases for higher equivalent Young's modulus, as shown in Fig. 2b. Nevertheless, for spheres whose diameter is 19.5 mm, contact strains for materials with equivalent Young's modulus in the range of $10 < E^* < 1000 \text{ MPa}$ are in the range of $10^{-2} < \epsilon_c < 5 \times 10^{-2}$, which are far from the range of small strains commonly adopted in geotechnical engineering. On the other hand, for materials with high Young modulus, such as rocks, this contact strain decreases to $\epsilon_c \approx 10^{-3}$.

In contrast, when the element in contact is a cylinder, the contact area is the entire flat surface of the cylinder. Therefore, the contact stress decreases significantly compared with the contact stress produced by a sphere. Moreover, the contact strain also decreases, and it is in the range of 10^{-6} to 10^{-4} , which fits better into the range of small strains.

The integration of the contact stresses on the loaded area using the Boussinesq solution, permits to obtain the distribution of vertical stresses, which gives an idea about the thickness of the material involved in the test. Fig. 3 shows the distribution of stresses produced by a sphere resting on a soil having an equivalent Young's modulus of $E^* = 50 \text{ MPa}$. It is noticeable in Fig. 3 that, when using a sphere of 19.05 mm

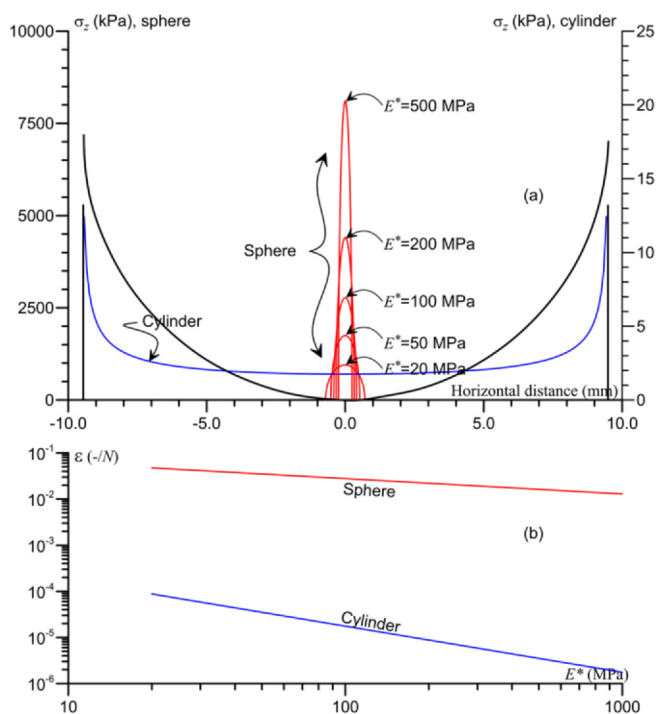


Fig. 2. (a) Contact stresses produced by spheres resting on materials of different equivalent Young's modulus E^* , or by a cylinder for a unit contact load $F_c = 1$ N; (b) surface strain in the symmetry axis.

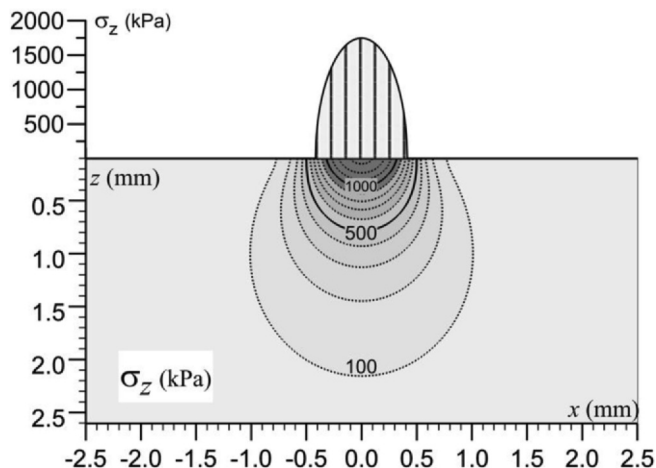


Fig. 3. Stresses produced by a sphere of 19.5 mm in diameter resting on a material having an equivalent Young's modulus of $E^* = 50$ MPa for a unit contact load $F_c = 1$ N.

in diameter, the penetration depth is only some millimeters.

On the other hand, when using a cylinder, vertical stresses in the material are smaller than when using a sphere, and the penetration depth, for a cylinder of 19.05 mm in diameter, increases to some centimeters, just as shown in Fig. 4.

The previous theoretical analysis of stress and strains produced by the contact of a sphere or a cylinder permits to examine the usefulness of the device when testing geomaterials. The following possibilities are imaginable depending on the strength and Young's modulus of the tested material:

- The use of a sphere as the contact element could not produce plastic strains in materials with high strength and high Young's modulus, such as rocks. Nevertheless, the strain in the contact point could be as high as 10^{-3} . Therefore, for a proper back-calculation, the

material must behave within the linear elastic domain up to this level of strain.

- In the case of intermediate materials, such as compacted fine soils or unsaturated natural materials, the net stress is not zero, even for zero total confining stress, because of the suction pressure. For this reason, those materials have some shear strength that can sustain contact stresses. However, as the suction pressure decreases, the high contact stress could surpass the strength of the material and, therefore, produce plastic strain. In this case, a sphere might not be appropriate as a contact element. Then, a cylinder with a flat surface could be a better option.
- Using a cylinder as a contact element reduces the contact stress significantly; therefore, it could be a good option even for cohesionless materials.
- Using a cylinder as a contact element ensures that the test applies small strains to the soil. However, the roughness of the tested material could be a difficulty that requires further analysis.

Experimental setup, material, and procedure

This section describes the experimental set up of the constructed device and the materials and procedures used in the different stages of this research. The properties of the material and samples vary in each stage due to the objective of each section. The first objective is to verify the correct operation of the developed equipment, so this stage uses control samples with known elastic properties.

After verifying the correct operation of the device, the measures obtained with rock and soil specimens are compared with the results obtained using conventional techniques reported in the literature. The following sections describe the device, the procedure carried out to verify its operation, as well as the material and procedures to test rock samples and compacted materials.

Description of the solitary stress wave device (SSW) and the experimental setup

The SSW device consists of a chain of steel spheres placed in a vertical position and struck by another sphere. A dynamic piezoelectric load cell, inserted in the middle of the chain, permits to measure the propagation of the solitary wave. The proposed setup, shown in Fig. 5, has three components: i) the SSW device, ii) a signal amplifier, and iii) a data acquisition equipment (*i.e.*, a recording oscilloscope).

The internal structure of the SSW device has 17 elements: 16 of them are steel spheres with a 19.05 mm diameter, while the mid

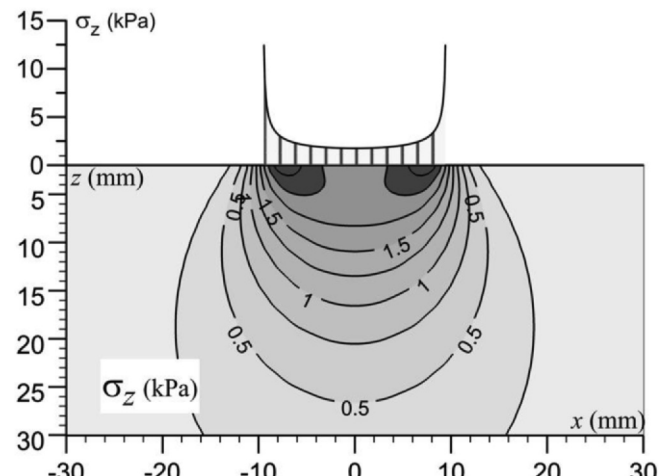


Fig. 4. Stresses produced by a cylinder of 19.5 mm in diameter resting on a material having an equivalent Young's modulus of $E^* = 50$ MPa for a unit contact load $F_c = 1$ N.

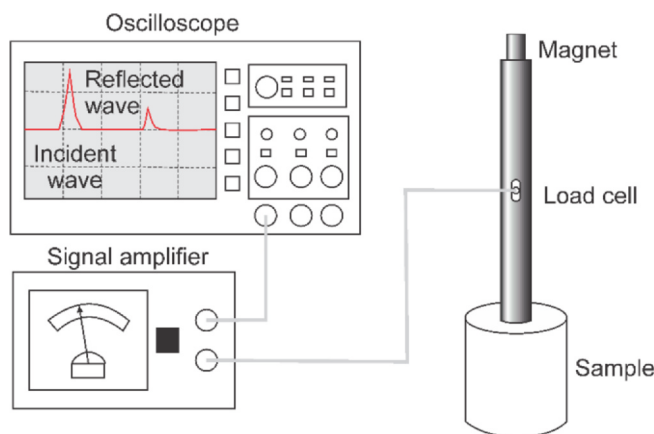


Fig. 5. Scheme of the Experimental.

element is a piezoelectric load cell, Omega DLC 101-100. The body of the device, shown in Fig. 6, has 19.06 mm internal diameter, and it is a Teflon tube coated with a 28.95 mm vinyl structure. The perturbation is produced at the top element by the strike made with a metallic sphere with a diameter of 19.05 mm. An electric magnet permits to attain a constant falling height of 6.6 mm, as proposed in [29].

Material and procedure on standard materials

The verification of the correct operation of the SSW device is possible by comparing the computed Young modulus obtained using the experimental values of the TOF and the relationships developed using the numerical model, with the Young modulus of the standard materials.

Two commercial polyurethane samples, similar to those used in previous works [13,14], were selected as control materials, as well as one sample of steel ASTM A36. Table 1 presents the values of the mechanical properties of those samples.

Material and procedures conducted on rocks samples

Eleven rock samples with bulk densities between 2050 and 2760 kg/m³, were tested using the SSW device. The device was placed on the center top surface of the cylindrical cored rock samples. During the experiments, the SSW test was repeated 3 times to compute the standard deviation of the modulus and its coefficient of variation, COV. After measuring the TOF using the SSW, the Young's modulus of the samples was calculated using the relationship obtained from the numerical model. Then, the actual Young's modulus of the rock specimens was computed by measuring the compressive wave velocity using ultrasonic transducers (*i.e.*, Proceq 325 40 177 P-wave Transducers). The assessment of Young's modulus using this wave velocity test was conducted according to [32].

Materials and procedure conducted on compacted soil samples

Two clayey soils were used to estimate the Young's modulus of compacted materials and to evaluate the performance of the SSW. These clays have high and low plasticity indexes, respectively (*i.e.*, PI = 55 and PI = 18). Samples were prepared under different compaction energies and water contents using the proctor standard hammer [33]; this procedure leads to different densities, as described in Table 2. Afterwards, the samples were extracted from the mold, and their TOF was measured on three different positions on their top surface.

For comparison, compression wave velocity was measured using ultrasonic transducers placed on the top and bottom of the sample. The first arrival method was used to measure the travel time of the wave

[34]. The ultrasonic wave velocity test on soil samples was conducted according to the method used in [35].

Materials and procedures conducted on compacted soil samples using the modified SSW device

Eleven soil samples were prepared and tested to verify the performance of the modified device. Nine of them were high plasticity clay with 31% of water content compacted using a strain-controlled press, reaching bulk densities between 1.56 and 1.80 g/cm³. Another sample, with a lower Young's modulus, was prepared from a slurry of the same clay beginning at a water content of 1.5 times the liquid limit and then consolidated to 50 kPa. One more sample was a mixture of sand and clay compacted to reach a bulk density of 1.83 g/cm³.

The Young's modulus of these samples was measured using the modified SSW. As in the previous sections, 3 tests were conducted on the surface of each sample. Using the results of the experimental TOF and the relations developed in the numerical model, the COV of the Young modulus measured with the modified SSW can be computed.

The dynamic shear rheometer (DSR apparatus, see Fig. 7) was selected in this stage as a reference test to cope with the inaccuracies of the wave velocity tests. Indeed, due to the different methods to measure the arrival time of the compressive wave, wave velocity tests lead to different estimations of the Young modulus [34]. The DSR is an apparatus currently used to measure the shear properties of liquid asphalt and other viscous materials. However, due to its high precision and the possibility of using a solid geometry, it was successfully used in [37] to measure the shear modulus of compacted soils and its dependence on the effective stress. As shown in Fig. 4, DSR tests are similar to dynamic torsional shear tests on solid cylindrical specimens, but they allow obtaining measurements with very high precision and in a broad frequency range [36,37]. In this research, DSR tests were carried out using cylindrical cored samples of 13 mm of diameter and variable height extracted from the original sample. The selected frequency of the torsional signal was 1 Hz, and the strains were in the range of 5×10^{-6} to 4×10^{-5} . The Young's moduli of the specimens were calculated using the DSR results (that provide the shear moduli), the degree of saturation of the sample, and the relationship suggested in [38,39] that gives the

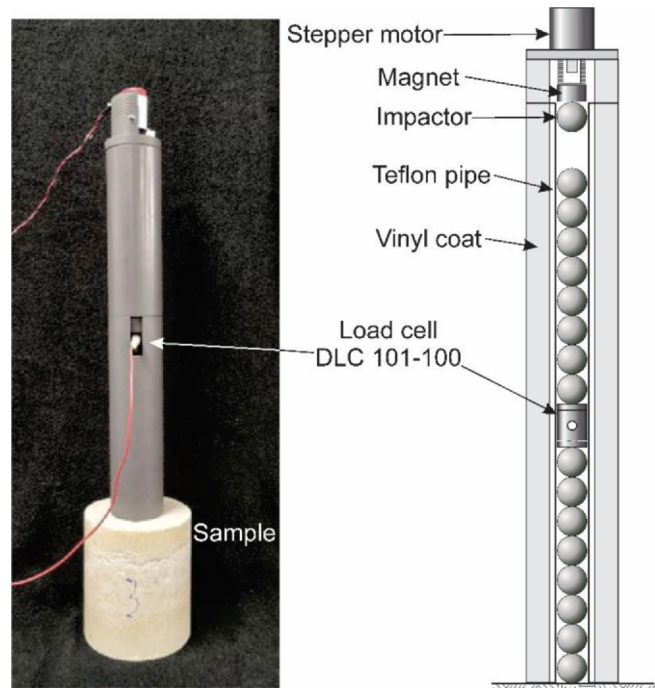


Fig. 6. Scheme of the developed SSW device.

Table 1

Mechanical properties of the control materials.

Material	Density (kg/m ³)	Young's Modulus (MPa)	Poisson's ratio	References
Soft polyurethane (SAWBONES 1522-03)	320	210	0.30	[30]
Hard polyurethane (SAWBONES 1522-04)	640	759	0.30	
Steel ASTM A36	7800	200,000	0.26	[31]

Poisson's ratio depending on the degree of saturation. See reference [37] for more details on DSR measurements in compacted soils and on the effect of suction on the shear modulus.

Results and discussion

This section presents the results of the three sets of tests. First, the results obtained on standard materials are described; this stage aims to explore the accuracy of the numerical procedure that simulates the operation of the device. After proving the proper operation of the device, the results on rock samples are presented and analyzed. Rocks were selected because they remain in the elastic domain during the test, and because there are reliable techniques for measuring their Young's modulus. Then, the device is challenged to measure the Young's modulus of soil samples. Although the results suggest a good empirical relationship between TOF and Young's modulus, there are significant differences between the experimental and the numerical TOF. These differences justify a modification of the device to distribute the stresses in a broader area, avoiding plastic deformations on the sample. The results obtained with the modified device resulted in values more similar to those obtained through the numerical model.

Results on standard materials

The first step to verify the performance of the device consisted of using the numerical model for comparing the elapsed time of the force recorded by the load cell and the force computed in element 9 of Fig. 1. These results are presented in Fig. 8. The results show a good agreement between the measured signal and the numerical solution (both forces normalized by their first peak value). It is observed that the differences between the measured and the computed TOF decrease as the underlying material becomes more rigid. Indeed, these differences are 40 µs for the soft polyurethane, 30 µs for the hard polyurethane, and 13 µs for the steel. In this figure, it can be observed that the second peaks are smaller in the experimental results than in the numerical results. The reason for this difference is that the losses of energy are not considered into the motion equations.

Furthermore, the results show that TOF has an inverse relation with the Young modulus. Fig. 9 depicts this inverse relation for different Poisson's ratios obtained in the numerical model. From this figure, it is also evident that the Poisson's ratio has a small effect in the computation of the Young's modulus. Indeed, the curves for different Poisson's ratios remain close to each other.

Fig. 9 includes grey dots that represent the Young's modulus of the standardized samples and the experimental TOF. It is important to notice that these points fall close to the computed lines. Despite the small differences between the numerical and experimental TOFs, the

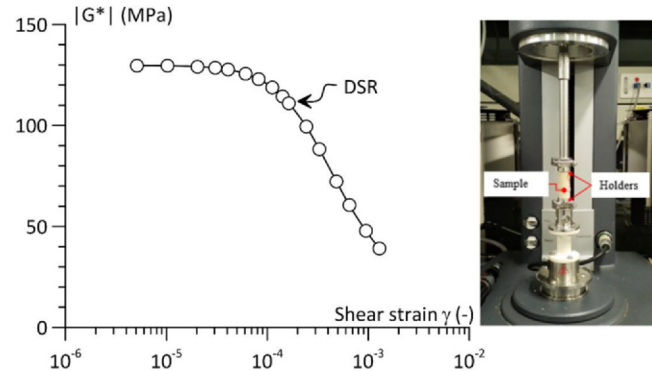


Fig. 7. Measure of the shear modulus of compacted soils using the dynamic shear rheometer DSR [37].

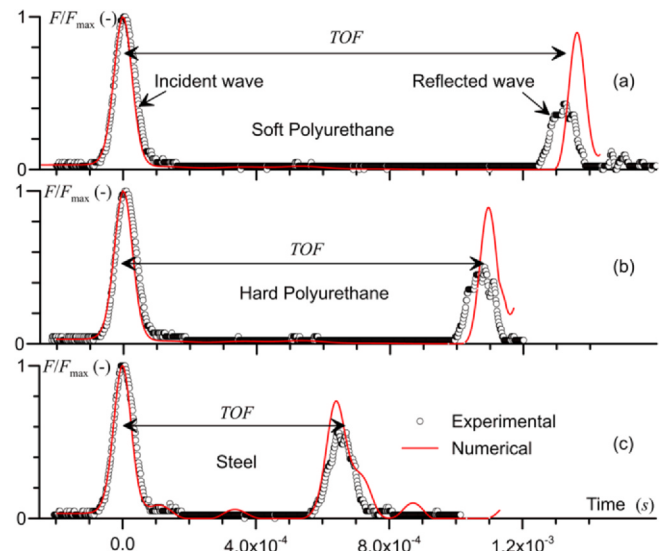


Fig. 8. Comparison between the results of the numeric simulation and the experimental values on control samples.

differences in Young's modulus grow compared with differences in TOF. Indeed, as shown in Table 3, differences in Young modulus are 22.6% for the soft polyurethane, 19.3% for the hard polyurethane, and 29% for the steel sample. These differences highly contrast with the discrepancies encountered in the TOF of 3.75%, 2.93% and 2.06% for the soft and hard polyurethane, and the steel sample. Fig. 10, which shows the derivative of the Young theoretical modulus with respect to TOF

Table 2

Characteristics of the compacted soil samples.

Number of Samples	Plastic Index	Compaction Energy (Blows)	Water Content (%)*	Bulk Density (g/cm ³)
4	55	25	25.3, 28.0, 37.7 and 35.0	1.61 to 1.77
5	18	12	21.1, 22.7, 23.1, 24.0 and 25.0%	1.85 to 1.90
4	18	25	17.8, 19.6, 20.6 and 22.3%	1.93 to 2.00
4	55	35	25.1, 27.8, 31.4 and 33.7%	1.70 to 1.80

* Water content was measured immediately after the test in a layer of 10 mm thick below the contact point.

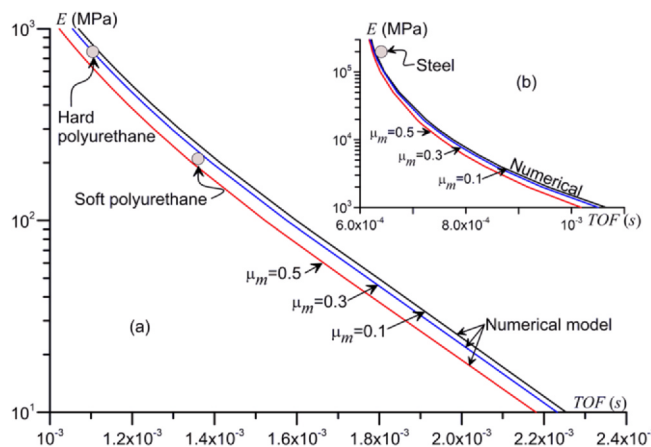


Fig. 9. Curves of Young's modulus numerically calculated. The dots represent the actual values of the Young modulus of the standardized materials.

(i.e., $\partial E / \partial \text{TOF}$), is useful to explain this increased discrepancy. For instance, for a Young's modulus of 1000 MPa and a Poisson's ratio of 0.3, an error in the measure of TOF of 1.0 μs leads to an error in the back-calculation of the Young modulus of 5.5 MPa. Therefore, as shown in Table 3 for the hard polyurethane, an error of 30 μs in the measure of the TOF leads to an error of around 165 MPa in the estimation of the Young's modulus. Moreover, for a given uncertainty in the TOF, the error in the back-calculation increases as the Young modulus grows.

Nevertheless, it is essential to remark that the comparisons made in Table 3 use the reference Young's modulus provided by the manufacturer without information on the strain level corresponding to such values. As polyurethane is a polymeric material, it does not behave as a linear elastic material. Therefore, a more precise evaluation of the Young's modulus of the reference materials and its dependency to strain could be useful for the comparison. However, this evaluation is beyond the scope of this research.

Results on rock samples

Fig. 11 compares the Young's modulus of rock samples obtained by measuring the TOF along with the numerical relationship (E_{SSW}), and the Young's modulus measured using the compressional wave velocity test (E_{UWV}) [32]. The curve giving the best fit through the origin practically overlaps the equality line $E_{\text{UWV}} = E_{\text{SSW}}$, with a correlation coefficient of 0.988, which leads to presume that both techniques are equivalent. Besides, the maximum COV of the three measurements per sample is 0.13, which also leads to conclude that there is an adequate repetitiveness of the measurements.

Results on soil samples

Fig. 12 compares the results of Young's moduli carried out on compacted soil samples measured with the wave velocity test (E_{WV}) and the moduli measured with the SSW device (E_{SSW}). The error bars in this figure represent the standard deviation of three measurements obtained with the SSW on the same sample. Additionally, the maximum COV computed from the Young's modulus obtained with the SSW is 0.28. Although the measurements suggest the possibility of an empirical

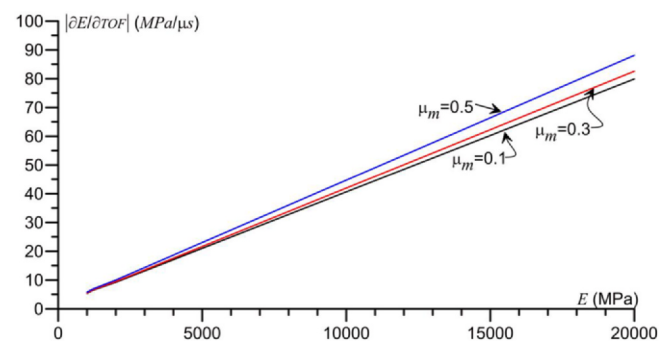


Fig. 10. Derivative of the theoretical relationship giving Young's modulus regarding TOF.

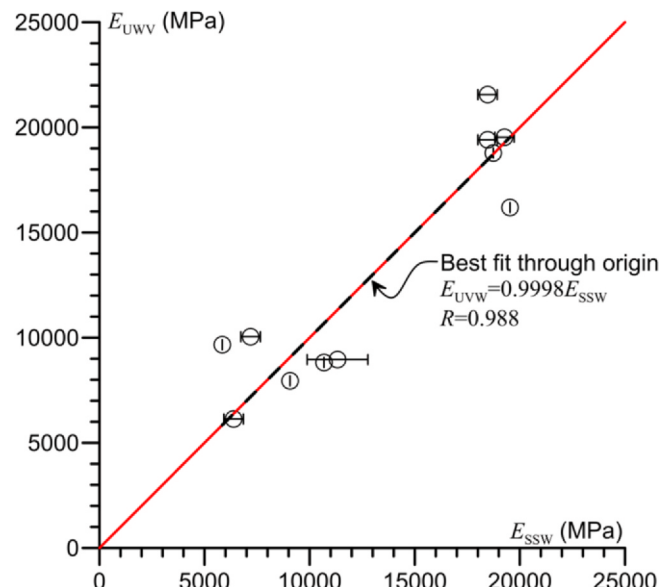


Fig. 11. Comparison of the Young modulus of rocks measured using ultrasonic wave velocities (E_{UWV}) and the SSW procedure (E_{SSW}). Horizontal lines represent error bars based on the standard deviation of three measures.

linear relationship between the moduli obtained using the wave velocity test and the SSW device, with a correlation coefficient of 0.97, this line falls apart from the equality line (i.e., $E_{\text{WV}} = E_{\text{SSW}}$) which is based on the numerical model. Furthermore, the disagreement between both methods is significant for Young moduli between 10 MPa and 650 MPa. As an example, the values of the Young's modulus measured with the wave velocity test are 1.423 times larger than those values obtained with the SSW.

Two sources of error can explain this difference:

1. Plastic deformations that appear at the contact between the last sphere and the tested material.
2. Inaccuracies of the wave velocity test caused by different methods to measure the arrival time, which leads to different estimations of the Young's modulus [34].

Table 3

Comparison of experimental and numerical simulation of TOF and Young modulus on control samples.

Material	Num. TOF (s)	Exp. TOF (s)	TOF % Diff.	Specified E (MPa)	Computed E (MPa)	E % Diff.
Soft polyurethane	1.36×10^{-3}	1.32×10^{-3}	3.75%	210	263.42	22.6%
Hard polyurethane	1.10×10^{-3}	1.07×10^{-3}	2.93%	759	921.41	19.3%
Steel	6.30×10^{-4}	6.43×10^{-4}	2.06%	2.0×10^5	1.42×10^5	29.0%

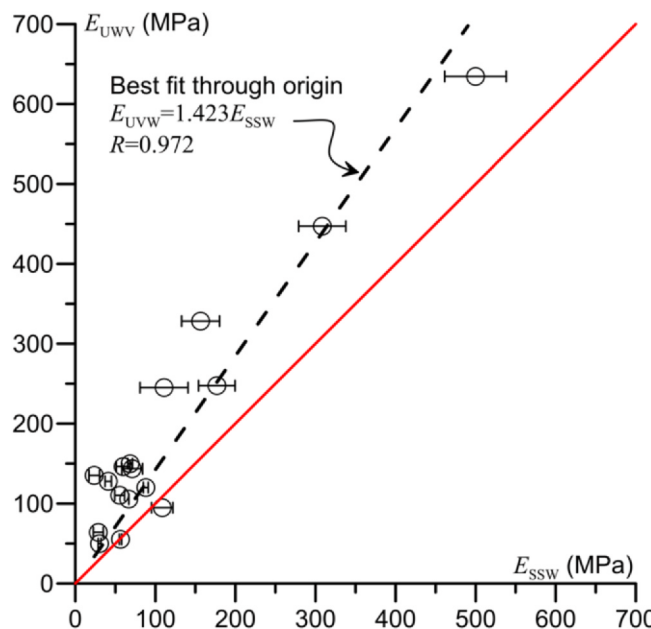


Fig. 12. Comparison of the Young modulus of compacted soils measured using ultrasonic wave velocities (E_{UWW}) and the SSW procedure (E_{SSW}). Horizontal lines represent error bars based on the standard deviation of three measures.

The first problem leads to discrepancies on the measured *TOF* compared with the numerical model because it assumes a Hertzian contact, for which all the materials must remain into the elastic domain. Therefore, an increase of the experimental *TOF* due to this plastic deformation leads to an underestimation of the Young's modulus.

An additional soil sample was compacted to a dry density of 1.851 g/cm³ and water content of 21.3% to verify the repetitiveness of the test procedure. Five solitary waves were applied to this sample at 1-minute intervals, measuring the *TOF* of each wave. The results show that the *TOF* standard deviation is 31 μ s. Although this is a small variation, it could increase the uncertainty in the subsequent calculation of the Young's modulus, as it is evidenced in the horizontal error bars of Fig. 12.

Results on soil samples using the modified SSW

Fig. 13 shows the results of the numerical simulation obtained by substituting the last contact equation from a sphere to a cylinder. The relationships between *TOF* and Young modulus in this figure are calculated for Poisson's ratios of 0.1 and 0.5.

The shear modulus obtained with the DSR is transformed into Young's moduli using the theory of linear elasticity and the values of the Poisson's ratio depending on the degree of saturation suggested in [38,39]. However, as DSR tests are carried out at a frequency of 1 Hz, they need to be corrected to take into account the effect of the frequency. Indeed, as shown in Fig. 8, the period of the stress signal applied by the SSW device is 4×10^{-4} s, which corresponds to an excitation frequency of 2500 Hz. The effect of the frequency on the shear moduli on the same compacted material of this study was assessed in [38], showing a linear increase of the shear modulus, on a logarithmic scale, of 5% for each decade interval of frequency. Consequently, for a frequency of 2500 Hz, the correction factor required for the measures at 1 Hz is estimated as 17%.

Fig. 13 also shows the experimental values of *TOF* obtained with the modified SSW and Young's moduli computed from the DSR measurements. This figure also shows an acceptable agreement with the numerical model. Fig. 14 allows comparing the results of Young's modulus obtained with both techniques (*i.e.*, the DSR and the SSW). The dashed line representing the linear fitting of the measurements has a

correlation coefficient of 0.95. This line is very close to the equality line, drawn in the figure with a solid line, which represents the equivalence between both techniques. This evidence suggests that the modified device could be used for testing compacted soil samples regardless of their softness.

Nevertheless, the horizontal bars in Fig. 14 show that some points have significant dispersion in the back-calculation of the Young's modulus; this dispersion is related to the dispersion in the *TOF* measurement. Performing the back-calculation based on the average *TOF* could cope with this difficulty, as is the case when using the bender element test. In fact, despite the large dispersion, the average value leads to good match with the comparative test, as shown in Fig. 14.

Conclusions

This research presents a new application of a nonlinear solitary strain wave device (SSW) on geo-materials. A modification of the proposed device is studied to reduce plastic deformation encountered on soil samples. The results presented in this paper permit to conclude the following regarding the performance of the device:

There is a good agreement between the measured and the computed time of flight or *TOF*. This time is defined as the time required by the wave to travel from the sensor and return after hitting the surveyed medium. Based on the obtained results, it is presumable that it is adequate to use the developed numerical solution for computing the Young's modulus of the tested samples.

Young's modulus computed with the results of the SSW device on elastic materials, such as rocks, showed good agreement when compared with the Young's modulus assessed from the standardized method of compressive wave velocity. This observation allows to conclude that both techniques seem to be equivalent.

Regarding soft materials, such as compacted soils, the sphere in contact with the soil can produce plastic deformation during testing. This deformation increases the *TOF* and produces an underestimation of the Young's modulus. There are two possibilities to circumvent this problem:

The first possibility is to include in the numerical model an elasto-plastic contact law that allows describing in a better way the plastic strain of the soil during testing. Nevertheless, this option requires including yield stress as an additional fitting parameter, complicating the inverse analysis based on only one measure.

A second option, which was preferred in this work, was to modify the SSW device by placing a metallic cylindrical element instead of the last sphere that is in contact between the device and the tested material.

The results of the Young's modulus obtained with the modified set-

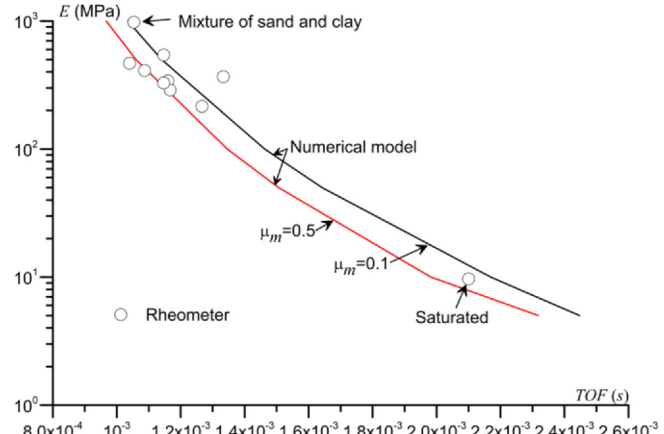


Fig. 13. Curves of Young's modulus calculated numerically for the modified SSW device (E) and values of Young's modulus of compacted materials measured using the DSR (dots symbols).

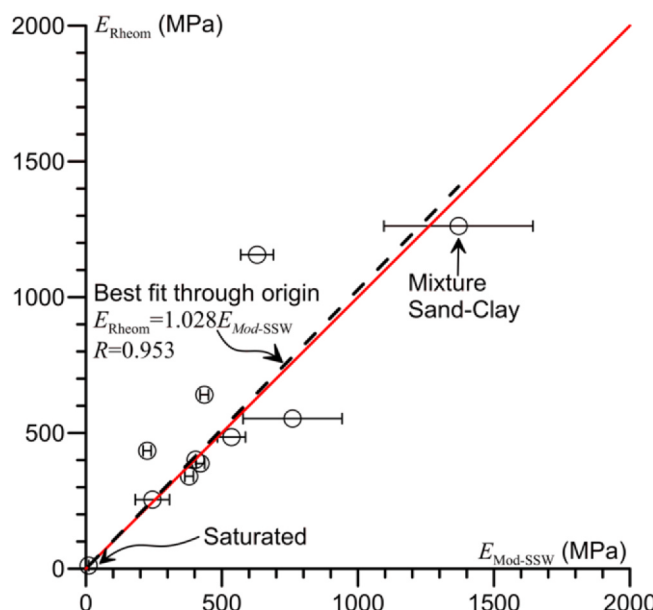


Fig. 14. A comparison between the moduli measured with the modified SSW ($E_{\text{Mod-SSW}}$) and the values assessed from the measures of the DSR (E_{Rheom}). Horizontal lines represent error bars based on the standard deviation of three measures.

up showed good agreement with the Young's modulus measured using a DSR, which is high-precision equipment.

Based on these results, it is possible to state that the SSW device could be a good nondestructive alternative for measuring the Young's modulus on geomaterials, both in-situ or in the laboratory.

However, the procedure and the results presented in this article are a first attempt of a feasibility study intending to use a solitary wave device to measure Young's modulus of geomaterials. This first work has several advantages and limitations, providing valuable information for future improvement.

One of the advantages of solitary waves is that they produce very clean waves allowing an easy peak-to-peak measure. Despite these clear waves, the measure of the elapsed time peak to peak leads to uncertainties of around $31 \mu\text{s}$ in the TOF, which induce uncertainties in the back-calculation of Young's modulus. The use of the cross-correlation technique could potentially reduce the dispersion in the measure of the TOF and, therefore, improve the calculation of Young's modulus.

The theoretical analysis of stress and strains produced by the contact of a sphere or a cylinder shows that the use of a sphere as the contact element could not produce plastic strains in materials that have high strength and Young's modulus, such as rocks. In contrast, intermediate materials, such as unsaturated materials, have some shear strength that can sustain contact stresses. Nevertheless, as suction decreases, the high contact stress could surpass the strength of the material and produce plastic strain.

The use of a cylinder as a contact element reduces the stress and increases the penetration depth of the test. However, the roughness of the tested material could be a problem that requires further analysis.

Another disadvantage of the proposed method is the uncertainty in the measure of the TOF, which leads to increased uncertainty in the back-calculation of the Young's modulus. Using the average TOF based on various measurements can overcome this shortcoming. Another possibility to reduce the dispersion in the TOF measurement could be the use of the cross-correlation technique.

This study uses a solitary wave device made with 16 steel balls of 19.5 mm of diameter, following the characteristics of the device proposed in [17]. As contact elements, this study uses either a steel sphere or a cylinder with a flat surface. However, for testing geomaterials, the

device could be optimized to reduce plastic strains when using a sphere or to avoid the problems related to the roughness of the surface of the tested material that appears when using a cylinder. Several variables could be included in such optimization include the number of elements, their material, and the magnitude of the impulse load. Besides, an optimization of the radius of the contact element could improve the penetration depth, avoiding plastic strains and reducing the effect of the surface roughness.

Funding

No funding was received for this work.

Intellectual Property

We confirm that we have given due consideration to the protection of intellectual property associated with this work and that there are no impediments to publication, including the timing of publication, with respect to intellectual property. In so doing we confirm that we have followed the regulations of our institutions concerning intellectual property.

Research Ethics

We further confirm that any aspect of the work covered in this manuscript that has involved human patients has been conducted with the ethical approval of all relevant bodies and that such approvals are acknowledged within the manuscript.

Declaration of Competing Interest

No conflict of interest exists.

References

- [1] ASTM D5311/D5311M-13 Test method for load controlled cyclic triaxial strength of soil. ASTM International; 2013.
- [2] Goto S, Tatsuoka F, Shibuya S, Kim Y, Sato T. A simple gauge for local small strain measurements in the laboratory. *Soils Found* 1991;31(1):169–80.
- [3] Caicedo B, Coronado O, Fleureau JM, Correia AG. Resilient behaviour of non standard unbound granular materials. *Road Mater Pavem Des* 2009;10(2):287–312.
- [4] Lings ML, Greening PD. A novel bender/extender element for soil testing. *Géotechnique* 2001;51(8):713–7.
- [5] Leong EC, Yeo SH, Rahardjo H. Measuring shear wave velocity using bender elements. *Geotech Test J* 2005;28(5):488–98.
- [6] ASTM D8296. Standard test method for consolidated undrained cyclic direct simple shear test under constant volume with load control or displacement control. West Conshohocken, PA: ASTM International; 2019.
- [7] Vucetic M, Lanzo G, Doroudian M. Damping at small strains in cyclic simple shear test. *J Geotech Geoenviron Eng* 1998;124(7):585–94.
- [8] Franke E, Kiekbusch M, Schuppener B. A new direct simple shear device. *Geotech Test J* 1979;2(4):190–9.
- [9] Airey DW, Wood DM. Discussion of “Specimen Size Effect in Simple Shear Test” by M. Vucetic and S. Lacasse (December, 1982). *J Geotech Eng.* 1984;110(3):439–42.
- [10] ASTM D4015-15e1. Test methods for modulus and damping of soils by fixed-base resonant column devices. ASTM International; 2015.
- [11] Drnevich V. Resonant-column testing—problems and solutions. In: *Dynamic Geotechnical testing*. ASTM International; 1978. p. 384–384–15.
- [12] Darraio C, Rizzo P. Method and apparatus for nondestructive evaluation and monitoring of materials and structures, U.S. Patent No. 8,327,709. 11 Dec. 2012.
- [13] Rizzo P, Li K. Analysis of the geometric parameters of a solitary waves-based harvester to enhance its power output. *Smart Mater Struct* 2017;26(7):75004.
- [14] Deng W, Nasrollahi A, Rizzo P, Li K. On the reliability of a solitary wave based transducer to determine the characteristics of some materials. *Sensors* 2015;16(1):5.
- [15] Nasrollahi A, Rizzo P, Orak MS. Numerical and experimental study on the dynamic interaction between highly nonlinear solitary waves and pressurized balls. *J Appl Mech* 2018;85(3).
- [16] Nguyen N-S, Brogliato B. Shock dynamics in granular chains: numerical simulations and comparison with experimental tests. *Granular Matter* 2012;14(3):341–62.
- [17] Schiffer A, Alkhaja AI, Yang J, Esfahani EN, Kim T-Y. Interaction of highly nonlinear solitary waves with elastic solids containing a spherical void. *Int J Solids Struct* 2017;118:204–12.
- [18] Schiffer A, Alia RA, Cantwell WJ, Lee D, Kim E, Kim T-Y. Elastic interaction between nonlinear solitary waves in granular chains and composite beams:

- Experiments and modelling. *Int J Mech Sci* 2020;170:105350.
- [19] Yang J, Silvestro C, Khatri D, De Nardo L, Daraio C. Interaction of highly nonlinear solitary waves with linear elastic media. *Phys Rev E* 2011;83(4):46606.
- [20] Ni X, Rizzo P, Yang J, Katri D, Daraio C. NDT & E International Monitoring the hydration of cement using highly nonlinear solitary waves. *NDT and E Int* 2012;52:76–85.
- [21] Popov VL. Contact mechanics and friction. Springer; 2010.
- [22] Nesterenko V. Dynamics of heterogeneous materials. Springer Science & Business Media; 2013.
- [23] Hertz H. Über die berührung fester elastischer Körper. *J für die reine und angewandte Mathematik* 1882;92:156–71.
- [24] Caicedo B. Geotechnics of roads: fundamentals. CRC Press; 2018.
- [25] Andreotti B, Forterre Y, Pouliquen O. Granular media. Cambridge University Press; 2013.
- [26] Sneddon IN. The relation between load and penetration in the axisymmetric Boussinesq problem for a punch of arbitrary profile. *Int J Eng Sci* 1965;3(1):47–57.
- [27] Zhai C, Gan Y, Hanor D, Proust G, Retraint D. The role of surface structure in normal contact stiffness. *Exp Mech* 2016;56(3):359–68.
- [28] Tran Tri V, Tucker-Kulesza Stacey E, Bernhardt Michelle. Soil surface roughness and turbidity measurements in erosion testing. IFCEE. 2018. p. 506–15.
- [29] Murillo C, Caicedo B, Thorel L. A miniature falling weight device for non-intrusive characterization of soils in the centrifuge. *Geotech Test J* 2009;32(5):465–74.
- [30] Sawbones Europe AB. Product catalogue 2002. Sawbones Europe AB; 2002.
- [31] ASTM A36/A36M - 19 Standard Specification for Carbon Structural Steel.
- [32] ASTM D-24845. Standard test method for laboratory determination of pulse velocities and ultrasonic elastic constants of rock. ASTM International; 2008.
- [33] ASTM D698 - 12e2 Standard Test Methods for Laboratory Compaction Characteristics of Soil Using Standard Effort (12 400 ft-lbf/ft³ (600 kN·m/m³)).
- [34] Murillo C, Sharifpour M, Caicedo B, Thorel L, Dano C. Elastic parameters of intermediate soils based on bender-extender elements pulse tests. *Soils Found* 2011;51(4):637–49.
- [35] Yesiller N, Inci G, Miller CJ. Ultrasonic testing for compacted clayey soils. In: Advances in Unsaturated Geotechnics, 2000, pp. 54–68.
- [36] Caro S, Beltrán DP, Alvarez AE, Estakhri C. Analysis of moisture damage susceptibility of warm mix asphalt (WMA) mixtures based on Dynamic Mechanical Analyzer (DMA) testing and a fracture mechanics model. *Constr Build Mater* 2012;35:460–7.
- [37] Villacreses JP, Caicedo B, Caro S, Yépez F. A novel procedure to determine shear dynamic modulus and damping ratio for partial saturated compacted fine-grained soils. *Soil Dyn Earthquake Eng* 2020;131:106029.
- [38] Oh WT, Vanapalli SK. Relationship between Poisson's ratio and soil suction for unsaturated soils. In: Proc., 5th Asia-Pacific Conf. on Unsaturated Soils. Kasetsart Univ. Bangkok, Thailand, 2011a, p. 239–245.
- [39] Oh WT, Vanapalli SK. The relationship between the elastic and shear modulus of unsaturated soils. In: Alonso E, Gens A. editors. Unsaturated soils, proceedings of the 5th international conference on unsaturated soils, 2011b, p. 341–46.